Award Number:
W81XWH-10-1-0766

TITLE: “Computational Model of the Eye for Primary and Secondary Blast Trauma”

PRINCIPAL INVESTIGATOR:
Thao D. Nguyen

CONTRACTING ORGANIZATION:
Johns Hopkins University
Baltimore, MD 21218

REPORT DATE: October 2015

TYPE OF REPORT:
Annual

PREPARED FOR: U.S. Army Medical Research and Materiel Command
Fort Detrick, Maryland 21702-5012

REPORT DOCUMENTATION PAGE

Form Approved
OMB No. 0704-0188

PLEASE DO NOT RETURN YOUR FORM TO THE ABOVE ORGANIZATION.

1. REPORT DATE *(DD-MM-YYYY)*	2. REPORT TYPE	3. DATES COVERED *(From - To)*
October 2015	Annual	28Sep2014 - 27Sep2015

4. TITLE AND SUBTITLE

"Computational Model of the Eye for Primary and Secondary Blast Trauma"

5a. CONTRACT NUMBER

5b. GRANT NUMBER
W81XWH-10-1-0766

5c. PROGRAM ELEMENT NUMBER

6. AUTHOR(S)
Bahram Notghi, Rajneesh Bhardwaj, Thao D. Nguyen

email:vicky.nguyen@jhu.edu

5d. PROJECT NUMBER

5e. TASK NUMBER

5f. WORK UNIT NUMBER

7. PERFORMING ORGANIZATION NAME(S) AND ADDRESS(ES)
Johns Hopkins University
Baltimore, MD 21218

8. PERFORMING ORGANIZATION REPORT NUMBER

9. SPONSORING/MONITORING AGENCY NAME(S) AND ADDRESS(ES)
U.S. Army Medical Research and Materiel Command
Fort Detrick, Maryland 21702-5012

10. SPONSOR/MONITOR'S ACRONYM(S)

11. SPONSOR/MONITOR'S REPORT NUMBER(S)

12. DISTRIBUTION/AVAILABILITY STATEMENT

Approved for Public Release; Distribution Unlimited

13. SUPPLEMENTARY NOTES

14. ABSTRACT
In the fifth year of the project, we focused on improving the computational model of the eye. The current eye model includes all important internal features of the eyes. The local thickness variations of important load-bearing ocular components (cornea and sclera) which are obtained based on published histological measurements have been included in our model. The findings of our simulations support experimental observations of injury to choroid, sclera, ciliary zonlues and ONH. The effect of local thickness variation have been investigated on the stress distribution, internal ocular pressure and estimated risk of injuries. We showed that using non uniform thickness for sclera-cornea shell changes the maximum von Mises stress in sclera, limbus and zonules of zinn. We have also improved our material model by adding a distributed fiber model to describe the anisotropic elastic behavior of the sclera and cornea based on published wide-angle X-ray scattering measurements of the anisotropic collagen structure.

15. SUBJECT TERMS
finite element analysis, risk of injuries, cornea, sclera, fluidstructure interaction

16. SECURITY CLASSIFICATION OF:			17. LIMITATION OF ABSTRACT	18. NUMBER OF PAGES	19a. NAME OF RESPONSIBLE PERSON
a. REPORT	b. ABSTRACT	c. THIS PAGE			USAMRMC
U	U	U	UU	31	19b. TELEPHONE NUMBER *(Include area code)*

Reset

Contents

1 Introduction

The increase use of explosive weaponry in military conflict and terrorist attack in recent years, has increased the number of combat related injuries sustained by soldiers and civilian induced by the blasts. The rate of ocular traumatic injuries to all injuries during the World War II become approximately 6 times larger in compare to the Operation of Desert Storm [1, 2, 3, 4], which make the ocular injuries as a fourth most common military deployment related injury [5]. The traumatic injuries due to a blast event, can be induced by four potentially injurious mechanisms; primary from the blast overpressure, secondary from propelled fragments, tertiary from blunt impact, and quarternary [6, 7]. While secondary, tertiary, and quarternary injury mechanisms are readily diagnosed and managed within the military's casualty care system, specific injury mechanisms unique to primary blast are one of the concern to ophthalmologists [8]. The severity of primary eye injury are correlated with the high-pressure shock front and the subsequent wave of lower sub-atmospheric pressure[9], threshold overpressure [10], reflection of the shock wave by the orbit [11, 12, 13], and facial features around the eye [14]. There is, however, a dearth of clinical data that could verify the hypotheses above and establish the mechanism of the injury. Measuring and assessing the influence of these factors is difficult because survivable primary blast injuries are likely accompanied by injuries from fragments and blunt force trauma and are thus more difficult to distinguish and enumerate. Moreover, the severity of the blast injuries and distance of the tertiary care facility from the injury site means that often patients are unable to recount the injury event, and witnesses are unavailable.

Hines-Beard et al. [15] tested the effects of blast overpressure on mice, by firing short bursts of pressurized air through paintball gun barrels, which inflicted closed eye injuries with features similar to those seen in patients with ocular blast trauma. Alphonse et al. [16] studied the effect of low-pressure blasts from fireworks and gunpowder charges on human cadaver eyes but reported chances of only minor corneal abrasion due to material projected from the fireworks during explosion. Risk of severe, physiological ocular damage was found to be less than 0.01% in this study [16]. Sherwood et al. [17] studied the anatomic features of primary blast ocular injury observed by using a postmortem porcine eye model exposed to various levels of blast energy. Bhardwaj et al. [14] demonstrated the effect of facial features on the blast loading of the eye and evaluated the ocular biomechanical

response to blast loading while taking into account the propagation of the acoustic wave inside the eye and the associated ocular deformation. Due to the importance of the facial features on the profile of the pressure induced by blast and challenges to performing the experimental studies in full scale, computational modeling can improve the understanding of the mechanism of the primary injuries. Computational models have been used recently to understand the mechanism of the primary blast injuries of the eye, induced by blast overpressure. Stitzel and Weaver [18] developed an in-house finite element model for blast loading on human eye, which used the pressure on the eye obtained as a function of mass of TNT charge and its distance from the subject. Rossi et al. [7] tested the dynamic response of the eye to blast overpressure and aimed to explain damage to the macula and optical nerve head due to the setting up of a standing wave inside the ocular orbit. Esposito et al. [19] proposed a computational model that presented the effects of peak overpressure and blast duration on macular trauma and expressed the possibility of severe damage of ocular tissues subjected to compression and traction loading.

To this end, a computational model which include the main internal ocular structures, spatially varying thickness of cornea-sclera shell and tissue properties, have been utilized to help us in understanding the mechanism of primary injuries and also provide a a measurable estimation of risk of injuries by using the risk of injuries developed by Brozoski et al.[20].

2 Body

2.1 Methods

A coupled fluid-structure interaction (FSI) solver [14] that employ the following methods have been used:

• Finite difference compressible flow solver for the propagation of the blast wave.

• Finite element elastodynamic solver with finite deformation of the human eye.

• Sharp-interface immersed boundary method for fluid-structure interaction.

The details of the above three main components of the modeling can be found in [14]. In this study the blast was modeled for the "base model" which will be described in section (2.1.1) is considered as a 2-kg TNT (Trini-

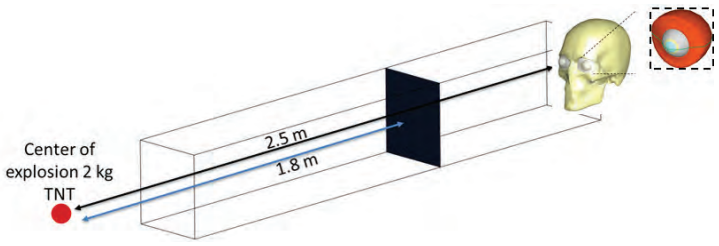

Figure 1: a Computational domain and initial conditions of the simulation for the blast directly in front of the face

trotoluene) explosion in front of the face, at a distance of 2.5 m from the face. These parameters are obtained based on the conditions of field tests for blast exposure, conducted by the US Army Research program [21]. The initial conditions for the blast in all simulations were identical to those used in [14]. The details of the explosion models can be found in [14]. A schematic of the initial condition of the blast is shown in the figure 1.

2.1.1 FE models of the head and eye

To characterize the deformation of the globe resulting from the blast wave, the FE model of the head developed by Rajneesh et al. [14], in which the eyelid and skin were neglected (referred to as "skull model") has been used. The anthropometric parameters of a specific 21-year-old male, given in Weaver et al.[22] is employed. The specific anthropometric data used for developing the skull model can be found in Ref. [14]. As it is shown in Fig. 2 the model includes all important internal features of the eyes including scleral, limbus, cornea, aqueous humor, lens, ciliary zonule, ciliary muscles, vitreous humor, retina, choroid, lamina cribrosa, pre-laminar neural tissue and the surrounding orbital/fatty tissue. The friction between the various ocular components, and the skull, were not consider and they fitted together seamlessly. This model was described in detail in the annual report for 2013.

The corneo-scleral shell is the outer, fibrous layer of the eye that protects the various intraocular components and is the main load bearing of the eyes. The corneo-scleral shell, exhibit significant regional variations in thickness, and in order to have accurate representation of the behavior of the eye under blast loading, these variations should be taken into account. In current study, the sclera is constructed based on the data obtained from high-field micro

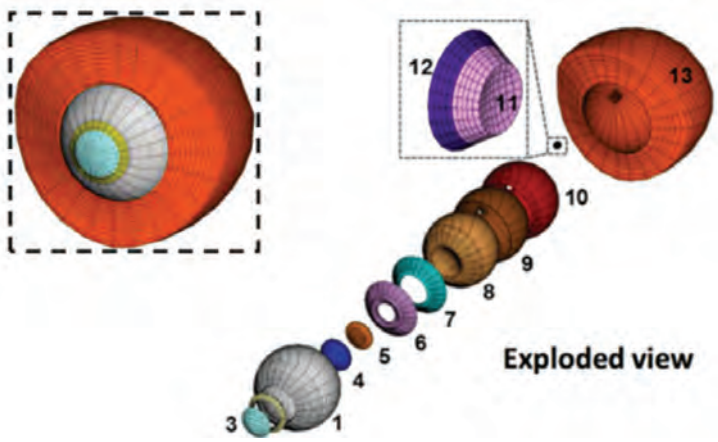

Figure 2: Ocular components in exploded view with associated zone numbers as described in Table 1, (Inset) Assembled view of the eye depicting the extraocular tissues, sclera, limbus and cornea.

Table 1: Zone numbering of different components

Component	Zone number
Sclera	1
Limbus	2
Cornea	3
Aqueous	4
Lens (Nucleus, Cortex)	5
Ciliary Zonule	6
Ciliary Muscle	7
Vitreous	8
Retina	9
Choroid	10
PLNT	11
LC	12
Extraocular tissue	13

MRI measurements performed by Norman et al. [23]. The corneal thickness is assumed to increase linearly from the apex to the limbus. In the model proposed by Stitzel et al. [24], corneal thickness was reported as 0.52 mm at the corneal apex and 0.66 mm at the limbus. In order to have a linear transition in thickness between tissue, the limbus is modeled as part of the cornea. The retinal and choroidal complexes were treated as shells of uniform thickness, terminating posteriorly at the ONH. The retina runs anteriorly up to the ora serrata, while the choroid extends up to the ciliary body. The retina thickness considered as 0.24 mm, which was reported by Wagner-Schuman et al. [25] for caucasian males. The choroid thickness reported as 0.35 mm by Ikuno et al. [26], based on measurements of mean sub-foveal choroidal thickness for healthy, Japanese individuals, with a mean age of 39 years. The lamina cribrosa (LC) is an extension of the peripapillary sclera, which is a mesh-like, multilayered network of collagen fibers that fit into the scleral canal wall, and allow the passage of nerve fibers and a central retinal artery into the globe. LC was modeled as a disc from a spherical section of thickness 0.45 mm, based on measurements for healthy eyes, by Jonas et al. [27]. The sections of the retinal and choroidal shells, adjacent to the LC, were grouped as the prelaminar neural tissue (PLNT). The PLNT is similar to retinal tissue, consisting of nerve fibers. Similar to the LC, the PLNT was modeled as a spherical section disc of thickness 0.59 mm (retinal thickness + choroidal thickness).

2.1.2 Material properties

There is a dearth in the literature describing the dynamic tests and mechanical behavior of ocular tissue subjected to blast impact. To best of our knowledge, literature containing the mechanical properties of ocular tissue subjected to blast impact experiments is very limited. In the present study, all ocular components were treated as Neo-Hookean solids and the best available material properties, available in literature were used. The density of the sclera was taken as 1,400 kg/m^3 (Stitzel et al.[24]), and the bulk modulus were calculated based on the measured speed of sound in the sclera [28], as 3570 MPa. The dynamic shear modulus of the sclera was taken as 10 MPa, based on the high strain rate measurements of Bisplinghoff et al. [29]. The density of the cornea is reported as 1150 kg/m^3 by Esposito et al.[19] and the bulk modules is reported as 3020 MPa by Steinert et al. [30]. The shear modulus of cornea obtained by inverse method is reported by Esposito et al. [19]

as 1.66 MPa. The properties of limbus considered to be the same as cornea. The density and bulk modulus of ciliary zonule and ciliary muscle considered the same as those reported for the lens. The value for the shear modulus are calculated based on the reported elastic modulus by Van Alphen et al. [31] as 119 Pa. The density of the aqueous and vitreous humor were reported by Duck et al. [32] as 1,003 and 1,009 kg/m3, respectively. Shear modulus for the vitreous humor considered as 7 Pa, based on the quasi-steady measurements of the shear modulus of bovine vitreous by Nickerson et al. [33] and the shear modulus of aqueous considered the same as that of vitreous. The density of both nucleus lens and cortex lens, considered as 1100 kg/m3 (Esposito et al. [19]) and the bulk modulus of both nucleus lens and cortex lens is calculated based on the measured speed of sound in the lens (Steinert et al. [30])as 2950. Shear modulus of nucleus lens and cortex lens was taken as 39 Pa and 98.3 Pa, from the [19]. Retinal density is considered as 1100 kg/m^3, as reported by Esposito et al. [19]. Due to lack of veritable data, and since the retina is composed mainly of cellular tissues and nerve fibers, the retinal bulk modulus was approximated the same as water (2265 MPa). The Young's modulus of retinal tissues exhibits large variations([34, 35]). The shear modulus of retina is considered as 3.51 kPa which is average value of the estimated shear modulus of porcine retina (3.35-3.67 kpa) with using contact angle measurement of a spreading droplet reported by Grant et al. [36]. The material parameters for choroid considered as those for the retina. The Young's modulus for lamina cribrosa was reported as 0.3 MPa by Norman et al.[37], considering Poisson's Ratio of 0.47, the shear modulus was calculated as 0.102 MPa. Density of the PLNT considered the same as the density of retina. The Young's modulus and Poisson's ratio of the PLNT obtained based on mean value of the ranges prescribed by Sigal [38] which lead to the shear modulus as 17.3 kPa. The properties for the extraocular tissues and orbital fat were taken as those reported for orbital fat. The density and bulk modulus were assumed to be equal to those of water 1000 kg/m3 and 2202 MPa, respectively ([39, 40, 41]). The shear modulus of orbital fat was taken as 900 kPa from the measurements of Schoemaker et al. [42] for simian retrobulbar tissues. The properties of the ocular components, used in our simulations, are as summarized in Table 2.

Table 2: Material properties used for the various ocular components. w water, r retina, s sclera, l lens

Component	ρ (kgm^{-3})	Ref	K (MPa)	Ref	μ (KPa)	Ref
Sclera	1400	[24]	3571	[28]	1000	[29]
Limbus	1150	[19]	3020	[30]	1660	[19]
Cornea	1150	[19]	3020	[30]	1660	[19]
Aqueous	1003	[32]	2266	[32]	0.007	[33]
Nucleus Lens	1100	[19]	2950	[30]	0.039	[19]
Cortex Lens	1100	[19]	2950	[30]	0.0983	[19]
Ciliary Zonule	1000	l	2950	l	0.119	[43]
Ciliary Muscle	1100	l	2950	l	0.119	c
Vitreous	1009	[32]	2353	[32]	0.007	[33]
Retina	1100	[19]	2200	w	3.51	[36]
Choroid	1100	[19]	2200	w	3.51	[36]
PLNT	1100	r	3571	s	17.3	[38]
LC	1400	s	3571	s	102	[37]
Extraocular tissue	1100	w	2202	8	500	[42]

2.1.3 Results and Discussion

This section is organized as follows. First, the results of the simulations of the skull model to characterize the biomechanical deformation of the the eye caused by blast pressure loading are presented. In Section 2.1.4, the possible injuries caused by blast over pressure which are reported in literature are correlated with the maximum stress obtained in different ocular components and also the risk of injuries are calculated based on the injury risk available in literature.

The maximum principal stress and maximum intraocular pressure (IOP) show periodic behavior(Fig. 4 and Fig. 3). The overall increase in maximum principal stress and IOP are due to the time-varying pressure loading boundary condition, and the periodic behavior of the stress and IOP for ocular components forming the posterior wall of the globe can be explained by the wave propagation inside the orbit. Furthermore, in order to verify this hypothesis, a first order time scaling analysis of the wave propagation was performed, the detail can be found in [14]. The time period calculated from the simulation was around 0.06 ms (Fig. 4 and Fig. 3) which is the same order of magnitude as the time period calculated by the scaling analysis. Oc-

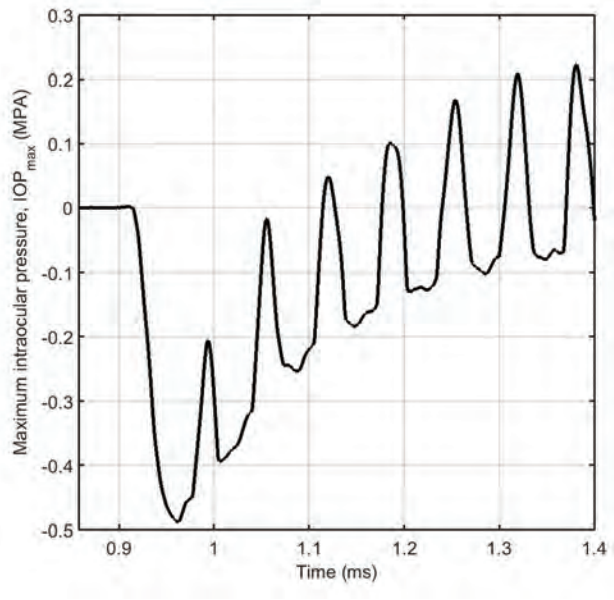

Figure 3: Time-varying maximum intraocular pressure (IOP).

ular components forming the posterior wall of globe, experience higher oscillatory tensile and compressive stress (Fig 3) and ocular components forming the anterior structures of globe quickly reached their peak principal stress and quickly decayed(Fig 5). Both trend of stress behavior agree with results reported by Rossi et al.[7].

The pressure inside the eye orbit was calculated as the mean of the three components of the principal stress. The maximum principal stress (S_1) and maximum pressure in 1.38 ms are shown in the transverse plane of the eye orbit in Fig. 7-a 7-b, respectively. The highest maximum principal stress is in thinnest part of sclera and the highest pressure can be noticed near the orbital wall due to the wave scattering by the orbital wall. The IOP was the highest in the posterior region of the vitreous. The contours of the von Mises stresses in the transverse plane are plotted in 7-c, in which the largest von Mises stresses appeared in the thinnest part of the sclera and near the optic nerve head. As it can be seen in Fig. 7-c, the sclera is distorted on the right side, due to asymmetric pressure loading.

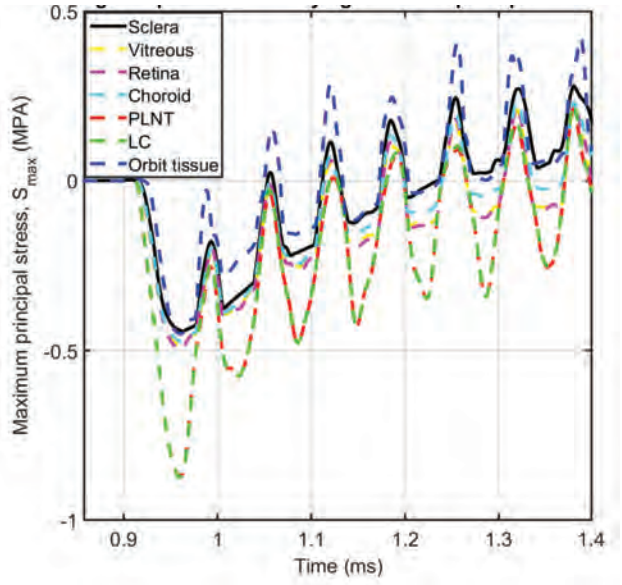

Figure 4: High amplitude time varying maximum principal stress

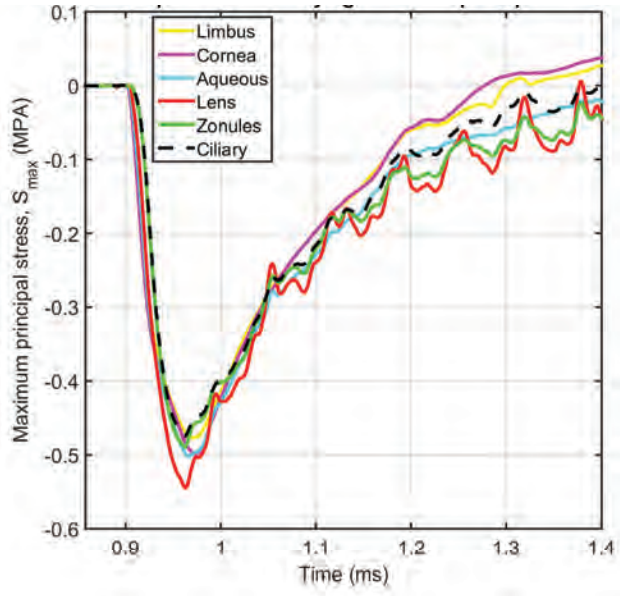

Figure 5: Low amplitude time varying maximum principal stress

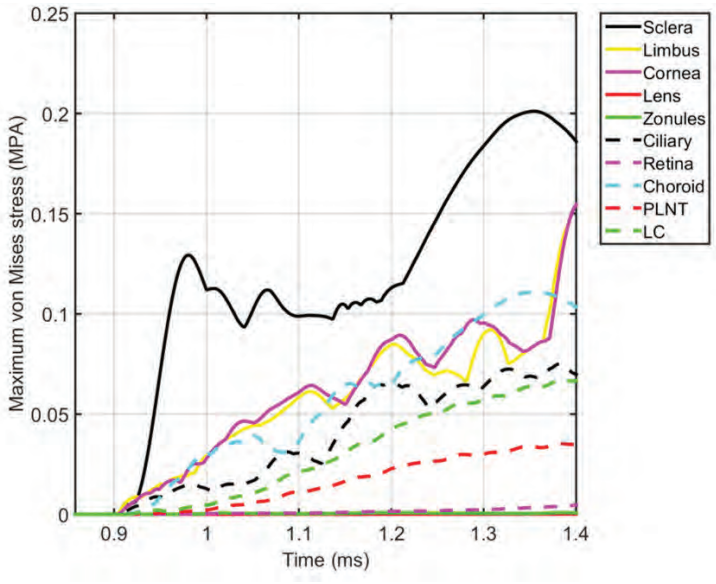

Figure 6: von Mises stresses shown in the transverse and sagittal plane for case 3

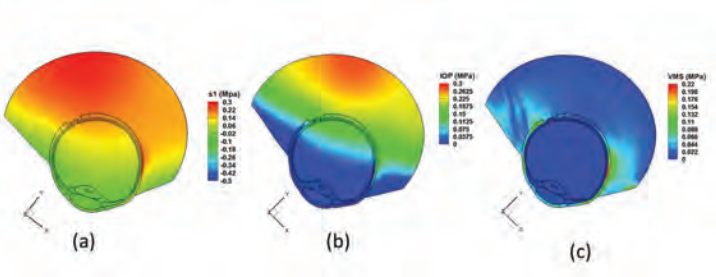

Figure 7: (a) Maximum principal stress in the transverse plane of the orbit.(b) Maximum pressure in the transverse plane of the orbit. (c) Maximum von misses stress in the transverse plane of the orbit.

2.1.4 Implications to the eye injury

As shown in Fig. 3 for the baseline case, the maximum IOP inside the globe reached 0.22 MPa, corresponding to around 1650 mmHg, which is two orders of magnitude larger than the 15 mmHg physiologic IOP for a healthy eye. The von Mises stresses were calculated largest in the sclera wall at the site of muscle attachments, which indicates possible risk of muscle tearing which agree with recent experiments of blast exposure on rats which have reported torn extraocular muscles (Hines-Beard et al.[15]). In addition, as shown in Fig. 6 the maximum von Mises stress in sclera, choroid and ciliary zonule show the possibility of internal scleral delamination (Sherwood et al.[17]), chorioretinal detachments (Rossi et al.[7], Sherwood et al. [17]), and lens dislocation (Stitzel et al.[24]).

We assessed the risk of eye injury using the functions published by Brozoski et al.[20] for blunt impact on the eye by a projectile. The injury risk function based on survival analysis with maximum likelihood is expressed as:

$$Injury\ risk = \left[1 - e^{-\frac{x^\beta}{\alpha^\beta}}\right] 100\% \tag{1}$$

where x is projectile normalized energy (kJ/m^2), β is a dimensionless parameter that depends on the injury type, and parameter α is expressed in terms of m^2/kJ. The values of α and β are obtained from the maximum likelihood parameter estimation technique for different types of eye injuries which were reported by Brozoski et al.[20]. Unfortunately, the authors did not report α and β for corneal abrasions. Consequently, the injury risk function based on logistic regression which is also developed by Brozoski et al.[20] were used to assess the risk for corneal abrasions:

$$Injury\ risk = \left[\frac{1}{1 + e^{\alpha - \beta x}}\right] 100\% \tag{2}$$

The maximum IOP obtained in our simulation with the projectile normalized energy for blunt impact. The correlation between the projectile normalized energy and IOP was reported by Duma et al. [44] for impact of different projectiles. We chose the correlation for the impact of 11.16 mm aluminum projectile because it is realistic representation of the exposed area of the eye that is affected by blast. The calculated percentage of injury risks corresponding to the maximum IOP value of 0.3 MPa for our simulation (baseline

Table 3: Injury risks calculated for model with uniform thickness (Uniform) and model with non-uniform thickness based on maximum IOP (MPa) using risk functions reported by [20], Cornea Abrasions calculated using logistic regression technique

Cases	Corneal Abrasions	Hyphema	Lens damage	Retinal damage	Globe rupture	Max IOP
Uniform	5	0.2	<0.01	<0.01	<0.01	0.22
Non-Uniform	4	0.1	<0.01	<0.01	<0.01	0.19

case) are approximately 4, 0.1, 0, 0, and 0% respectively, for corneal abrasions, hyphema, lens dislocation, retinal damage, and globe rupture.

The injury risk values for all cases are summarized in Table 3.

2.1.5 Sensitivity of the model to sclera thickness

In this section, in order to show the sensitivity of the response of the model with respect to variational change in thickness of the cornea-sclera shell, a comparison between the non-uniform and model with uniform sclera thickness is performed. The model with uniform thickness have constant 1 mm thickness for the sclera. The comparison of time-varying corneo-scleral maximum principalscleral maximum principal stress for non-uniform model and model with uniform thickness is shown in Fig. 9. The model with non-uniform thickness showed 8% increase in the maximum value of maximum principal stress and 3.5% increase in the average of maximum principal stress. The comparison of time-varying maximum IOP for non-uniform model and model with uniform thickness is shown in Fig. 8. The model with non-uniform thickness showed, 14% decrease in the maximum value of maximum IOP and 3.3% decrease in the average of maximum IOP in compare to uniform model. The injury risk values for the uniform model are summarized in Table 3. Even though, the maximum cornea-sclera shell stress and maximum IOP in both model have very similar trends in both models, however, as it is shown in Fig.10 (a), the average of maximum von Mises stress in cornea-sclera shell for non-uniform model is higher (25%) than uniform model. In addition,the average of maximum von Mises stress in ciliary and choroid for non-uniform model are higher 6% and 40 %, respectively and 4% lower in limbus.

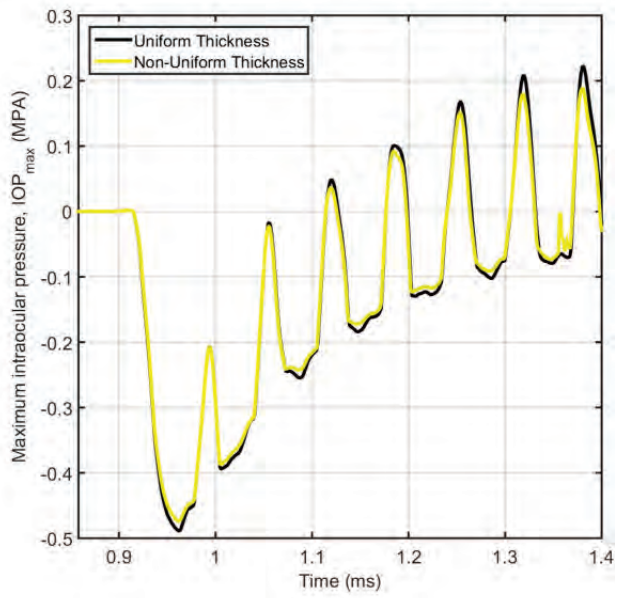

Figure 8: Comparison among four cases with different thickness for time-varying maximum intraocular pressure, IOP

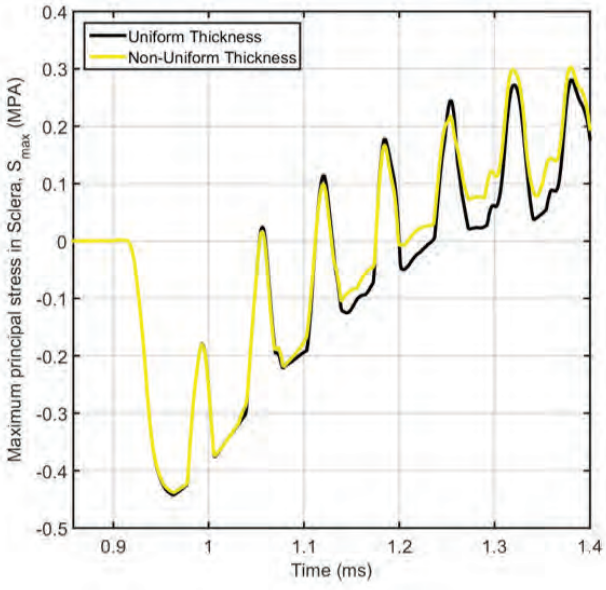

Figure 9: Comparison among four cases with different thickness for time-varying and corneo-scleral principal stress, s1

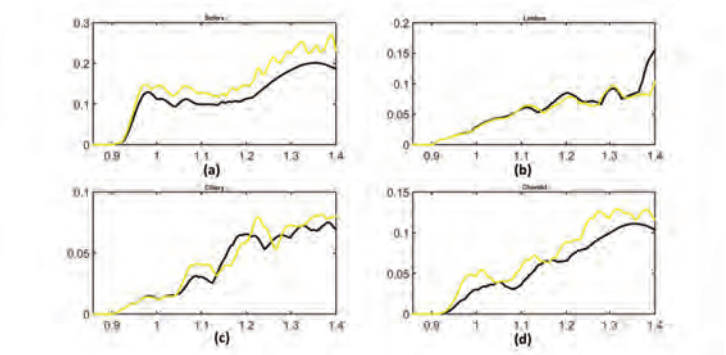

Figure 10: Comparison of time-varying maximum von Mises stress for (a)sclera, (b) limbus, (c) ciliary body, (d) choroid

3 Limitations of the computational model

In the present computational model, the tissues of the cornea and sclera were assumed to be isotropic and spatially homogeneous in the Neo-Hookean constitutive model, although Aghamohammadzadeh et al. [45] have demonstrated the anisotropic and non-linear behavior of the sclera. We are currently working on adding the anisotropy to the model. Although we have used the best available material properties for the ocular components, there may be uncertainty in the material properties at high blast loading rates. We also did not account for the viscoelastic nature of ocular tissue which can influence the stresses and IOP.

4 Work in Progress

We are currently working on incorporating collagen derived anisotropy of the cornea and sclera in the computational model to investigate their effects on the risk of injuries, deformation, stress response of the globe to the blast wave.

4.1 Anisotropic mechanical properties of the cornea and sclera

The mechanical properties of the sclera obtain from its fiber-reinforced microstructure, which consists of a stack of collagen lamellae, composed mainly of unidirectional type I collagen fibers embedded in a proteoglycan rich matrix ([46]). The collagen fiber structure of the posterior human sclera was recently investigated using wide-angle X-ray scattering (WAXS) (Pijanka et al. [47]). In WAXS, X-rays passing through the ordered fibrous collagen structure are scattered to produce a diffraction pattern. The quantification of corneal and scleral collagen fiber orientation from WAXS patterns can be found in detail in [48]. The WAXS measurements showed the existence of a ring of highly aligned collagen in the region closest to the ONH. the degree of anisotropy in the peripapillary ring varied markedly (between 2-fold and 4-fold) with circumferential position around the scleral canal and weakest circumferential alignment is observed in the superior-nasal quadrant [47]. The collagen structure in the midposterior sclera exhibited large variations in the preferred fiber orientations as well as a low degree of fiber alignment for this reason the rest of the sclera was considered as isotropic material in this study. In our study, as it is shown in Fig. 11 the peripapillary sclera is divided to 4 quadrant and different degree of anisotropy is assigned to each quadrant.

The material parameters for the cornea $(\mu, \beta, \alpha\ )$ is selected in way to match the uniaxial tests performed by Zeng et al. on human cornea [49]. The arrangement of collagen fibrils is important to determine the mechanical strength of the cornea. X-ray scatter intensity distribution data has indicated two preferred directions of collagen orientation at the center of the cornea: along the nasal-temporal and superior-inferior meridians([50, 51]). Closer to the limbus, the fibers tend to run in a circumferential direction [51]. In the center of the cornea, preferential orientations are dominant along the superior-inferior SI and the nasal-temporal NT meridians. At the limbus, where the cornea and the white sclera merge, most collagen fibrils are aligned circumferentially clearly forming a reinforcing annulus. The anisotropic material parameters are summarized in Table 4.

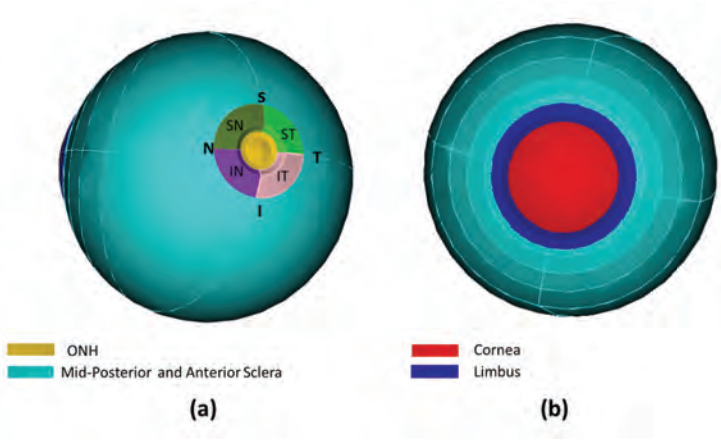

Figure 11: Cornea-sclera shell sections

Table 4: Anisotropic material parameters of cornea-sclera shell, MA, mid-posterior and anterior sclera; PP, peripapillary sclera; SN, superior-nasal quadrant; ST, superior-temporal quadrant; IN, inferior-nasal quadrant; IT, inferior-temporal quadrant.

Component	$\mu(KPa)$	α(Pa)	β	Ref	Fiber Anisotropy	Fiber Orientation	Ref
Sclera-MA	160	5.00E+02	215	[52]	0	0	[52]
Sclera-PP-SN	160	5.00E+02	215	[52]	0.45	0.74	[52]
Sclera-PP-ST	160	5.00E+02	215	[52]	0.68	0.74	[52]
Sclera-PP-IN	160	5.00E+02	215	[52]	0.59	0.74	[52]
Sclera-PP-IT	160	5.00E+02	215	[52]	0.54	0.74	[52]
Limbus	60	1.04E+05	4.45	Estimated	0.37	0	[53]
Cornea	60	1.04E+05	4.45	Estimated	0	0	[53]

4.2 Anisotropic hyperelastic constitutive model

The sclera and cornea, limbus was idealized as a continuum composite consisting of fiber families, each representing a collagen lamella with an in-plane orientation angle, ϕ, embedded in an isotropic matrix. The collagen structure was described by a continuous probability density distribution of the fiber orientations, D(ϕ). The matrix and collagen fibers deform with the tissue according to the macroscopic deformation gradient F, which maps a vector from the undeformed configuration to the deformed configuration. The invariants of the right Cauchy green tensor ($\mathbf{C} = \mathbf{F}^T\mathbf{F}$) are defined as follows:

$$I_1 = \mathrm{tr}(\mathbf{C}) \tag{3}$$

$$I_2 = \frac{1}{2}(\mathrm{tr}(\mathbf{C})^2 - \mathrm{tr}(\mathbf{C}^2) \tag{4}$$

$$I_3 = \det(\mathbf{C}) \tag{5}$$

The strain energy for component with this material model can be decomposed into a matrix term and an anisotropic term dependent on the fiber stretch which can be described as follow:

$$W(\mathbf{C}) = W_{matrix}(I_1(\mathbf{C}), I_2(\mathbf{C}), I_3(C)) + W_{aniso}(\mathbf{C}) \tag{6}$$

The collagen fibers assumed to be identical and can be described by using the same strain energy density

$$W_{fiber}(\lambda_f) = \frac{\alpha}{\beta}[\exp(\beta(\lambda_f^2 - 1)) - \beta\lambda_f^2] \tag{7}$$

Where $4\alpha\beta$ is stiffness of the fiber family and β is a strain stiffening parameter and λ_f is the stretch of the fiber determined by $\mathbf{C} : \mathbf{N}(\phi)$, where $\mathbf{N}$ is the unit vector describing the fiber orientation. The anisotropic

$$W_{aniso}(\mathbf{C}) = \int_{-\pi}^{\pi} W_{fiber}(\lambda_f(\phi))D(\phi)d\phi \tag{8}$$

The matrix phase was modeled as an isotropic,quasi-incompressible Neo-Hookean material.

$$W_{matrix}(I_1(C), I_3(C)) = \frac{\mu}{2}(I_1 - 3) + \frac{\kappa}{2}(I_3 - \ln(I_3) - 1) \tag{9}$$

where μ is shear modulus and κ is bulk modulus.

Table 5: The range of shear modulus for isotropic parameters sensitivity analysis

Component	Upper range (Pa)	Lower range(Pa)
Sclera	10^6	10^7
Cornea	1660×10^3	1660×10^4
Nucleus	25.2	52.8
Cortex	33.8	162.8
Retina and Choroid	2800	4200
Ciliary Zonule	95.44	143.16

4.2.1 Sensitivity of the model to the material properties and blast conditions

Sensitivity analysis will be performed to investigate the effect of material parameters and blast conditions (mass and distance of explosive) on stress response, maximum IOP and risk of injuries. The sensitivity analysis will be performed as follow.

Isotropic We are conducting a parameter study to understand the effect of material properties of the sclera, cornea, lens (nucleus, cortex), ciliary zonule, retina and choroid for isotropic model. The bulk moduli and density were not varied. The shear moduli of these components are considered as a variable in our sensitivity analysis. The shear modules of nucleus, cortex and the shear modules of retina, choroid considered to change together which reduce the number of variables of this study to 5 variables. In order to understand the effect of shear moduli on the maximum IOP and risk of injuries, a fractional factorial design is used to construct a 2^3 experiments which achieves resolution III design. The range of the variation, for nucleus and cortex considered as [25.2 52.8]Pa and [33.8 162.8]Pa, respectively, based on the values reported by [19]. The shear modulus of the corneo and sclera, varied from their base value to the 10 fold higher which is in the order of the scleral modulus measured for high-pressure rates [29]. The variation in shear modulus of ciliary zonule, retina and choroid considered as 20% of their nominal values which was reported in Table 2. The range of shear modulus are summarized in Table 5.

Table 6: Range of anisotropic material parameters of cornea sclera shell, MA, midposterior and anterior sclera; PP, peripapillary sclera; SN, superior-nasal quadrant; ST, superior-temporal quadrant; IN, inferior-nasal quadrant; IT, inferior-temporal quadrant.

Component	β	$\alpha\beta$ (KPa)	Fiber Anisotropy
Sclera-MA	[172 258]	[86 129]	0
Sclera-PP-SN			[0.37 0.52]
Sclera-PP-ST			[0.56 0.82]
Sclera-PP-IN			[0.49 0.70]
Sclera-PP-IT			[0.45 0.64]
Limbus	[3.56 5.34]	[370 555]	[0.33 0.40]
Cornea			0

Anisotropic A parameter study will be performed to investigate the effect of anisotropic material parameters of the cornea-sclera shell on the stress response and estimated risk of injuries. The bulk moduli and density were not varied. As it was described in section 4.1, different anisotropic parameters(preferred fiber orientation, degree of anisotropy) have been assigned to different section of cornea-sclera shell based on WAXS data. In order to understand the effect of anisotropic material parameters of cornea-sclera shell on the stress response and risk of injuries, a set of simulations, designed based on resolution III fractional factorial analysis, will be performed. The range of anisotropic material model for cornea sclera shell are summarized in Table 6.

Blast conditions The effect of the parameters of the blast on the injury risk and stress response in ocular component will be investigated as part of sensitivity analysis. The simulation will be performed with 0.64 and 6.4kg TNT blasts and the result will be compared to the base model. Based on the weight of the explosive charge used, the standoff distance (radius of the circle) was varied, such that conditions for 0% lethality and pulmonary injury threshold were emulated. [54]

4.2.2 Risk of Injuries

We are currently applying experimental data for blunt impact to asses the injury risks associated with the blast pressure. This likely leads to erroneous injury risk criteria because the IOP and stresses generated in the intraocular tissues by the propagating blast wave is very different for the same impact energy comparing blast to blunt impact. Blast events exposes the tissues to significantly higher rates and the high rate response of ocular tissues has been shown to be different than for low rates. There is currently no experimental data published for primary blast injury to ocular tissues. Sherwood and coauthors [55, 17] have begun to examine damage in cadaveric porcine eyes exposed to blast pressures generated by a shock tube. In future work, we will used their data to estimate the probability of sub-globe-rupture injuries under various blast pressure-impulse. Blast parameters will be used to estimate the likelihood of a specific type of injuries. A score based system will be used to determine the levels of trauma based on the blast pressure profile [17].

5 Key Research Outcomes

1. Developed a more detailed model of the human eye with internal ocular structures and spatially varying thickness.
2. IOP, VMS Mises stress and principal stresses were obtained in different component of the eye.
3. Risk of injuries were used to obtain the likelihood of specific injuries due to the blast.
4. The findings of our simulations support experimental observations of injury to choroid, sclera, ciliary zonule and ONH.
5. The effect of local thickness variation have been investigated on the stress response, internal ocular pressure and estimated risk of injuries.
6. Began to include the anisotropic material model to the cornea-sclera shell in order to describe the nonlinear, anisotropic stress response of the load bearing components of eye.
7. Began to estimate the effect of material parameters and blast conditions in the stress response of the eye and estimated risk of injuries

6 Conclusion

A FSI computational model was presented to investigate the effect of the blast wave on the human eye. The transient flow fields and pressure loading profile on the human eye were obtained by simulating the three dimensional blast wave propagation. The possible eye injuries and associated injury risks were estimated by using the calculated intra-ocular pressure (IOP) and von Mises stress in the various ocular components. The sensitivity of the model to local variation of the sclera were determined and discussed.

The future goals are to consider anisotropic material of the cornea-sclera shell and determine the effect of anisotropy on the stress response of the eye and estimated risk of injuries in our model. In addition, we will perform the parameters study (material parameters, blast conditions) to determine the effect of each parameters on the stress and estimated risk of injuries. A new damage criteria based on the blast parameters will be used to estimate the likelihood of a sub-globe-rupture injuries.

7 Publications, Abstracts and Presentations

1. S. Bailoor, R. Bhardwaj, T. D. Nguyen"Effectiveness of Eye Armor During Blast Loading", Biomechanics and Modeling in Mechanobiology, **14**:1227-37, 2015.

2. R. Bhardwaj , Ziegler K, Seo J. H, Ramesh K.T., Nguyen T.D"Computational Model of Blast Loading on the Human Eye", Biomechanics and Modeling in Mechanobiology, **13**:123-140, 2014.

3. B. Notghi, R. Bhardwaj, T. D. Nguyen, "Biomechanics of the Human Eye under Blast Loading", Summer Biomechanics, Bioengineering and Biotransport Conference, Snowbird, Utah, 2015.

4. S. Bailoor, A. K. Soti, R. Bhardwaj, T.D. Nguyen, "Biomechanics of the Human Eye under Blast Loading", 17th U.S. National Congress on Theoretical and Applied Mechanics, Michigan State University, East Lansing, Michigan, 6/17/2014.

5. S. Bailoor, A. K. Soti, R. Bhardwaj, T. D. Nguyen, "Effectiveness of Eye Armor During Blast Load", poster presentation, ASME Summer Bioengineering Conference, Sunriver, Oregon, WA, 6/26- 29/2013.

6. K. A. Ziegler, T. D. Nguyen, "Modeling study investigating the depth-dependent fiber reinforcement in corneal tissue", poster presentation Summer Bioengineering Conference, June 20-23th, 2012, Fajardo Puerto Rico.

7. R. Bhardwaj, K.A. Ziegler, T. D. Nguyen "Blast Wave Reflections on the Human Eye", poster presentation: ARVO, Fort Lauderdale, FL, May 9, 2012.

8. K.A. Ziegler, R.S. Yatnalkar, K.T. Ramesh, T.D. Nguyen "Modeling Study for the Design of an Innovative Composite Membrane Inflation Test", poster presentation: Summer Bioengineering Conference, June 22-25th, 2011, Farmington Pennsylvania.

9. R. S. Yatnalkar, K. A. Ziegler, K. T. Ramesh, T. D. Nguyen, "Development of a Shock Tube to Study Primary Blast Effects in Ocular Blast Injuries", Conference presentation: Society of Experimental Mechanics, June 14th, 2011, Uncasville, CT.

References

[1] W. STONE. Ocular injuries in the armed forces. Journal of the American Medical Association, 142(3):151–152, 1950.

[2] E. D. Weichel, M. H. Colyer, S. E. Ludlow, K. S. Bower, and A. S. Eiseman. Combat ocular trauma visual outcomes during operations iraqi and enduring freedom. Ophthalmology, 115(12):2235–2245, 2008.

[3] J. S. Heier, R. W. Enzenauer, S. F. Wintermeyer, M. Delaney, and F. P. LaPiana. Ocular injuries and diseases at a combat support hospital in support of Operations Desert Shield and Desert Storm. Archives of ophthalmology, 111(6):795–798, 1993.

[4] T. Y. Wong, G. S. Smith, A. E. Lincoln, and J. M. Tielsch. Ocular trauma in the United States Army: hospitalization records from 1985 through 1994. American journal of ophthalmology, 129(5):645–650, 2000.

[5] E. D. Weichel, M. H. Colyer, C. Bautista, K. S. Bower, and L. M. French. Traumatic brain injury associated with combat ocular trauma. The Journal of head trauma rehabilitation, 24(1):41–50, 2009.

[6] A. Kemper, V. Alphonse, C. McNally, I. Herring, P. Brown, J. Stitzel, and S. Duma. Response of Porcine Eyes to Blast Overpressure: Effects of Overpressure Severity and Boundary Conditions.

[7] T. Rossi, B. Boccassini, L. Esposito, C. Clemente, M. Iossa, L. Placentino, and N. Bonora. Primary blast injury to the eye and orbit: finite element modeling. Invest. Ophthalmol. Visual Sci, 53(13):8057–8066, 2012.

[8] A. B. Thach, A. J. Johnson, R. B. Carroll, A. Huchun, D. J. Ainbinder, R. D. Stutzman, S. M. Blaydon, S. L. DeMartelaere, T. H. Mader, C. S. Slade, et al. Severe eye injuries in the war in Iraq, 2003–2005. Ophthalmology, 115(2):377–382, 2008.

[9] D.-E. S. Concussion injuries. Text-book of Ophthalmology, volume vol VI: Injuries. London, Henry Kimptonm, 1954.

[10] R. Abbotts, S. Harrison, and G. Cooper. Primary blast injuries to the eye: a review of the evidence. Journal of the Royal Army Medical Corps, 153(2):119–123, 2007.

[11] H. HF. Primary blast injuries. Ind Med, page 3:142, 1973.

[12] R. Scott. The injured eye. Philosophical Transactions of the Royal Society B: Biological Sciences, 366(1562):251–260, 2011.

[13] W.-Y. M. Mechanics of blast injuries. 1945.

[14] R. Bhardwaj, K. Ziegler, J. H. Seo, K. Ramesh, and T. D. Nguyen. A computational model of blast loading on the human eye. Biomechanics and modeling in mechanobiology, 13(1):123–140, 2014.

[15] J. Hines-Beard, J. Marchetta, S. Gordon, E. Chaum, E. E. Geisert, and T. S. Rex. A mouse model of ocular blast injury that induces closed globe anterior and posterior pole damage. Experimental eye research, 99:63–70, 2012.

[16] V. D. Alphonse, A. R. Kemper, B. T. Strom, S. M. Beeman, and S. M. Duma. Mechanisms of eye injuries from fireworks. JAMA, 308(1):33–34, 2012.

[17] D. Sherwood, W. E. Sponsel, B. J. Lund, W. Gray, R. Watson, S. L. Groth, K. Thoe, R. D. Glickman, and M. A. Reilly. Anatomical Manifestations of Primary Blast Ocular Trauma Observed in a Postmortem Porcine ModelPrimary Blast Ocular Trauma. Investigative ophthalmology & visual science, 55(2):1124–1132, 2014.

[18] J. D. Stitzel and A. A. Weaver. Computational simulations of ocular blast loading and prediction of eye injury risk. In ASME 2012 Summer Bioengineering Conference, pages 425–426. American Society of Mechanical Engineers, 2012.

[19] L. Esposito, C. Clemente, N. Bonora, and T. Rossi. Modelling human eye under blast loading. Computer methods in biomechanics and biomedical engineering, 18(2):107–115, 2015.

[20] F. Brozoski, E. Kennedy, S. Duma, and S. Street. FINAL REPORT Eye Injury Risk Functions for Human and FOCUS Eyes: Hyphema, Lens Dislocation, and Retinal Damage. Update, 2011.

[21] K. L. McNesby, B. E. Homan, J. J. Ritter, Z. Quine, R. Z. Ehlers, and B. A. McAndrew. Afterburn ignition delay and shock augmentation in fuel rich solid explosives. Propellants, Explosives, Pyrotechnics, 35(1):57–65, 2010.

[22] A. A. Weaver, K. L. Loftis, J. C. Tan, S. M. Duma, and J. D. Stitzel. CT based three-dimensional measurement of orbit and eye anthropometry. Investigative ophthalmology & visual science, 51(10):4892–4897, 2010.

[23] R. E. Norman, J. G. Flanagan, S. M. Rausch, I. A. Sigal, I. Tertinegg, A. Eilaghi, S. Portnoy, J. G. Sled, and C. R. Ethier. Dimensions of the human sclera: thickness measurement and regional changes with axial length. Experimental eye research, 90(2):277–284, 2010.

[24] J. D. Stitzel, S. M. Duma, J. M. Cormier, and I. P. Herring. A nonlinear finite element model of the eye with experimental validation for the prediction of globe rupture. In SAE CONFERENCE PROCEEDINGS P, pages 81–102. SAE; 1999, 2002.

[25] M. Wagner-Schuman, A. M. Dubis, R. N. Nordgren, Y. Lei, D. Odell, H. Chiao, E. Weh, W. Fischer, Y. Sulai, A. Dubra, et al. Race-and sex-related differences in retinal thickness and foveal pit morphology. Investigative ophthalmology & visual science, 52(1):625, 2011.

[26] Y. Ikuno, K. Kawaguchi, T. Nouchi, and Y. Yasuno. Choroidal thickness in healthy Japanese subjects. Investigative ophthalmology & visual science, 51(4):2173–2176, 2010.

[27] J. B. Jonas, E. Berenshtein, and L. Holbach. Lamina cribrosa thickness and spatial relationships between intraocular space and cerebrospinal fluid space in highly myopic eyes. Investigative ophthalmology & visual science, 45(8):2660–2665, 2004.

[28] J. Bereiter-Hahn. Probing biological cells and tissues with acoustic microscopy. In Advances in acoustic microscopy, pages 79–115. Springer, 1995.

[29] J. A. Bisplinghoff, C. McNally, S. J. Manoogian, and S. M. Duma. Dynamic material properties of the human sclera. Journal of biomechanics, 42(10):1493–1497, 2009.

[30] R. F. Steinert. Cataract surgery. Elsevier Health Sciences, 2010.

[31] G. Van Alphen and W. P. Graebel. Elasticity of tissues involved in accommodation. Vision Research, 31(7):1417–1438, 1991.

[32] F. A. Duck. Physical properties of tissues: a comprehensive reference book. Academic press, 2013.

[33] C. S. Nickerson, J. Park, J. A. Kornfield, and H. Karageozian. Rheological properties of the vitreous and the role of hyaluronic acid. Journal of biomechanics, 41(9):1840–1846, 2008.

[34] K. Chen and J. D. Weiland. Anisotropic and inhomogeneous mechanical characteristics of the retina. Journal of biomechanics, 43(7):1417–1421, 2010.

[35] I. Jones, M. Warner, and J. Stevens. Mathematical modelling of the elastic properties of retina: a determination of Young's modulus. Eye, 6(6):556–559, 1992.

[36] C. A. Grant, P. C. Twigg, M. D. Savage, W. H. Woon, M. Wilson, and D. Greig. Estimating the mechanical properties of retinal tissue using contact angle measurements of a spreading droplet. Langmuir, 29(16):5080–5084, 2013.

[37] R. E. Norman, J. G. Flanagan, I. A. Sigal, S. M. Rausch, I. Tertinegg, and C. R. Ethier. Finite element modeling of the human sclera: influence on optic nerve head biomechanics and connections with glaucoma. Experimental eye research, 93(1):4–12, 2011.

[38] I. A. Sigal. Interactions between geometry and mechanical properties on the optic nerve head. Investigative ophthalmology & visual science, 50(6):2785–2795, 2009.

[39] S. Cirovic, R. M. Bhola, D. R. Hose, I. C. Howard, P. Lawford, J. E. Marr, and M. A. Parsons. Computer modelling study of the mechanism of optic nerve injury in blunt trauma. British journal of ophthalmology, 90(6):778–783, 2006.

[40] E. D. Power. A nonlinear finite element model of the human eye to investigate ocular injuries from night vision goggles. PhD thesis, Virginia Polytechnic Institute and State University, 2001.

[41] J. Al-Sukhun, C. Lindqvist, and R. Kontio. Modelling of orbital deformation using finite-element analysis. Journal of the Royal Society Interface, 3(7):255–262, 2006.

[42] I. Schoemaker, P. Hoefnagel, T. Mastenbroek, F. Kolff, S. Picken, F. van der Helm, and H. Simonsz. Elasticity, viscosity and deformation of retrobulbar fat in eye rotation. Investigative Ophthalmology & Visual Science, 45(13):5020–5020, 2004.

[43] M. Mikielewicz, R. Michael, G. Montenegro, L. Pinilla Cortes, and R. Barraquer. Elastic properties of human lens zonules as a function of age in presbyopes. Acta Ophthalmologica, 91(s252):0–0, 2013.

[44] S. M. Duma, J. A. Bisplinghoff, D. M. Senge, C. McNally, and V. D. Alphonse. Evaluating the risk of eye injuries: intraocular pressure during high speed projectile impacts. Current eye research, 37(1):43–49, 2012.

[45] H. Aghamohammadzadeh, R. H. Newton, and K. M. Meek. X-ray scattering used to map the preferred collagen orientation in the human cornea and limbus. Structure, 12(2):249–256, 2004.

[46] P. G. Watson and R. D. Young. Scleral structure, organisation and disease. A review. Experimental eye research, 78(3):609–623, 2004.

[47] J. K. Pijanka, B. Coudrillier, K. Ziegler, T. Sorensen, K. M. Meek, T. D. Nguyen, H. A. Quigley, and C. Boote. Quantitative mapping of collagen fiber orientation in non-glaucoma and glaucoma posterior human sclerae. Investigative ophthalmology & visual science, 53(9):5258, 2012.

[48] K. M. Meek and C. Boote. The use of X-ray scattering techniques to quantify the orientation and distribution of collagen in the corneal stroma. Progress in retinal and eye research, 28(5):369–392, 2009.

[49] Y. Zeng, J. Yang, K. Huang, Z. Lee, and X. Lee. A comparison of biomechanical properties between human and porcine cornea. Journal of biomechanics, 34(4):533–537, 2001.

[50] K. M. Meek, T. Blamires, G. F. Elliott, T. J. Gyi, and C. Nave. The organisation of collagen fibrils in the human corneal stroma: a synchrotron X-ray diffraction study. Current eye research, 6(7):841–846, 1987.

[51] K. M. Meek and R. H. Newton. Organization of Collagen Fibrils in the Corneal Stroma in Relation to Mechanical Properties and Surgical. Journal of Refractive Surgery, 15:695–699, 1999.

[52] B. Coudrillier, J. Pijanka, J. Jefferys, T. Sorensen, H. A. Quigley, C. Boote, and T. D. Nguyen. Collagen structure and mechanical properties of the human sclera: Analysis for the effects of age. Journal of biomechanical engineering, 137(4):041006, 2015.

[53] C. Boote, C. S. Kamma-Lorger, S. Hayes, J. Harris, M. Burghammer, J. Hiller, N. J. Terrill, and K. M. Meek. Quantification of collagen organization in the peripheral human cornea at micron-scale resolution. Biophysical journal, 101(1):33–42, 2011.

[54] S. Bailoor, R. Bhardwaj, and T. Nguyen. Effectiveness of eye armor during blast loading. Biomechanics and Modeling in Mechanobiology, 14(6):1227–1237, 2015.

[55] W. Gray, M. Reilly, B. J. Lund, W. E. Sponsel, and R. D. Glickman. Sub-lethal Ocular Trauma (SLOT): Establishing a Standardized Blast Threshold to Facilitate Diagnostic, Early Treatment, and Recovery Studies for Blast Injuries to the Eye and Optic Nerve. Technical report, DTIC Document, 2014.